Journal of
Composites Science

MDPI

Article

Synthesis and Characterization of Silicon–Carbon Powder and Its Resistance to Electron Irradiation

Vyacheslav Ivanovich Pavlenko [1], Natalia Igorevna Cherkashina [1,*], Oleg Dmitrievich Edamenko [1], Roman Nikolaevich Yastrebinsky [1], Anton Valerievich Noskov [2], Dmitry Stanislavovich Prokhorenkov [1], Andrey Ivanovich Gorodov [1] and Anastasia Olegovna Piskareva [1]

[1] Department of Theoretical and Applied Chemistry, Belgorod State Technological University Named after V.G. Shukhov, 308012 Belgorod, Russia; belpavlenko@mail.ru (V.I.P.); kafnx@mail.ru (O.D.E.); yrndo@mail.ru (R.N.Y.); bstu-cvt-sem@yandex.ru (D.S.P.); gorodov-andreyy@mail.ru (A.I.G.); a.burdasova@inbox.ru (A.O.P.)
[2] Department of Theoretical and Experimental Physics, Belgorod State National Research University, 308015 Belgorod, Russia; noskovbupk@mail.ru
* Correspondence: cherkashina.ni@bstu.ru

Abstract: The issue of crystallization of silicon oxide at low temperatures is a topical issue for the electronics of the future. Organosilicon oligomers and polymers are "ideal" sources for obtaining ultrapure silicon ceramics and silicon nanoparticles. This paper presents the results of the synthesis of highly dispersed silicon-carbon powder from an organohydrosiloxane oligomer and the method for increasing its crystallinity at low temperatures. The diffraction pattern of the resulting powder corresponds to the amorphous–crystalline state of the components in this material, as evidenced by two intense and broadened amorphous halos in the region of Bragg angles 2θ = 7–11° and 18–25°. The resulting silicon–carbon powder was subjected to electron irradiation (E = 10 MeV; D = 10^6–10^7 Gy). This paper presents the data on the changes in powder properties via IR-Fourier spectroscopy, X-ray phase analysis, and scanning electron microscopy. Irradiation with fast electrons with an absorbed dose of 10^6 Gy leads to a slight crystallization of the amorphous SiO_2 phase. An increase in the absorbed dose of fast electrons from D = 10^6 to D = 10^7 Gy leads to the opposite effect. An amorphization of silica is observed. This study showed the possibility of the crystallization of a silicon–carbon powder without a significant increase in temperature, acting only with electron irradiation. It is necessary to continue further research on expanding the boundaries of the optimal doses of absorbed radiation from fast electrons in order to achieve the maximum effect of the crystallization of silicon–carbon powder.

Keywords: composite powder; silicon–carbon powder; electron irradiation; crystallization

Citation: Pavlenko, V.I.; Cherkashina, N.I.; Edamenko, O.D.; Yastrebinsky, R.N.; Noskov, A.V.; Prokhorenkov, D.S.; Gorodov, A.I.; Piskareva, A.O. Synthesis and Characterization of Silicon–Carbon Powder and Its Resistance to Electron Irradiation. *J. Compos. Sci.* **2023**, *7*, 340. https://doi.org/10.3390/jcs7080340

Academic Editor: Francesco Tornabene

Received: 2 August 2023
Revised: 14 August 2023
Accepted: 18 August 2023
Published: 20 August 2023

1. Introduction

In recent years, researchers have paid great attention to obtaining non-oxide and oxide ceramics from organosilicon oligomers and polymers of various classes, which are widely used in aviation and cosmic engineering products [1–3]. The traditional methods of manufacturing Si-based ceramics are built on solid-phase synthesis and are highly energy intensive. For example, as a result of the solid-phase reaction of SiO_2 with carbon, SiC silicon carbide is obtained at about 2500 °C.

Organosilicon polymers already contain Si, O, and C in their molecular chain in the form of alkyl, allyl, or aryl groups, usually with methyl CH_3- and ethyl C_2H_5- groups. The structure of linear polyorganosiloxanes contains the ready-made fragments of $(\equiv Si\text{-}O\text{-}Si\equiv)_n$ polymeric chain structures necessary to create nanoscale amorphous silica.

Obtaining silicon-containing RD ceramics is due to the presence of a strong Si-C chemical bond in the molecules of the corresponding oligomers and polymers, which prevents the removal of carbon in the form of low molecular weight carbohydrates during

pyrolysis in an inert environment. However, the final ceramic product is usually obtained at a temperature of about 1100 °C.

Thus, organosilicon oligomers and polymers are "ideal" sources for obtaining ultrapure silicon ceramics and silicon nanoparticles [2,4].

In practice, organochlorosilanes of the general formula (R_xSiCl_{4-x}), polyorganosilanes whose main chain consists of silicon atoms (≡Si-Si≡) with side organic substituents, polyorganocarbosilanes (containing Si-C, Si-Si bonds), polyorganosiloxanes of the general formula $R_xSi(OR^1)_{4-x}$ (where R and R^1 are organic groups), tetraethoxysilanes of the general formula $Si(OR)_4$, and others are used as initial silicon compounds for ceramics production [5].

From the scientific and practical point of view, an important issue is the influence of the carbon structure on the crystallization ability of amorphous silica produced from organosilicon oligomers and polymers. Currently, there is no consensus on this issue [6–8].

The widespread use of SiO_2-based coatings and highly dispersed powders has determined a variety of alternative methods for obtaining SiC and SiCO compounds.

There is a variety of methods of synthesis of films and highly dispersed powders based on SiO_2 and carbon-containing mineral phases, as well as methods of amorphous silica crystallization [4–16]. These include electron-beam, plasma-arc, pulsed photonic methods, laser annealing, chemical vapor deposition, high-temperature, metal-induced, and sol–gel methods.

One promising method of creating the system (SiO_2 | C) is the modification of silica via a high-energy beam of fast electrons to form Si clusters, which are highly chemically active. Exposure to fast electrons can lead to the transformation of amorphous silica into a crystalline phase. The advantage of the electron-beam modification of materials is that the electron beam can be focused into a spot of less than 10 nm, i.e., it is possible to change the properties of silica on the nano-scale.

The authors of this work were the first who used a non-polar organosilicon liquid linear oligomer of polyalkylhydrosiloxane as a precursor, widely used in practice as a hydrophobizer of glass, metal ceramics, fabrics, and other products.

The solution to the problem of the low-temperature synthesis of crystalline SiO_2-based films and coatings from organosilicon liquid polyalkylhydrosiloxane will make it possible to create a cheap radiation-resistant ceramic microcomposite in the dielectric-semiconductor system.

The purpose of this work is to obtain highly dispersed crystalline SiO_2 in the presence of carbon phase from liquid polyalkylhydrosiloxane oligomer under the influence of thermal pyrolysis and irradiation with fast high-energy electrons.

2. Materials and Methods

2.1. Sample Preparation

Polyalkylhydrosiloxane liquid (Point LLC, St. Petersburg, Russia) was used for the synthesis of the silicate-carbon (SC) powder. Hydrophilic silicate-carbon (SC) powder was synthesized via pyrolysis (300 °C) of organohydrosiloxane oligomer with high content of active hydrogen in the siloxane chain (Si-H). SC is a white powder with the following properties: bulk density 0.45 g/cm^3, true density 2.01 g/cm^3, and specific surface 3.5 m^2/g. Figure 1 shows the energy spectrum of the SC material. The atomic average composition determined using energy-dispersive X-ray spectroscopy (EDS) is shown in Table 1.

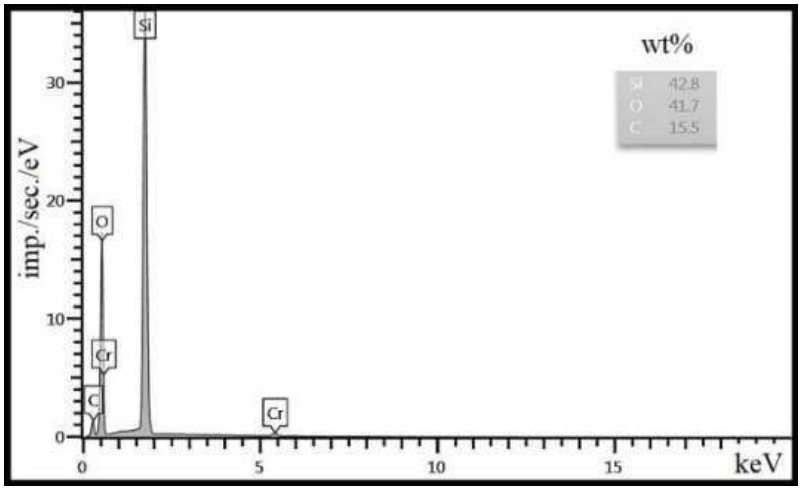

Figure 1. Energy spectrum of the SC material according to the results of EDS.

Table 1. Atomic composition of the SC material, % wt.

Si	O	C
42.8	41.7	15.6

Ready SC-material (hereinafter referred to as material) was subjected to ultrasonic treatment in aqueous-alcohol solution using ultrasonic generator U-840 (frequency 35 kHz, N = 0.95 kW) with the subsequent drying.

2.2. Research Methods

2.2.1. Electron Irradiation

Irradiation of compressed material samples in the form of a cylindrical tablet (diameter 23 mm, height 5 mm) was carried out using an industrial unit of a high-frequency electron linear accelerator UELR-10-15S1. Pulsed electron beam power is 15 kW, operating frequency is 2856 MHz, scanning bandwidth is 400 mm, electron fluence is 3.5×10^{15} electron/cm^2·s), single absorbed dose is 10–20 kGy (1 Gy = 1 J/kg) depending on the time (1–2 s) the material was in the chamber. The value of absorbed doses in the studied material was 10^5, 10^6, and 10^7 Gy. The calculated heat flux density on the surface of the material was about 100 W/mm^2. The calculated surface heating of the target was ~1250 °C. The temperature of the irradiated material samples did not exceed 150 °C. The temperature was controlled using a MEGEON 16450 (ARCO Electronics Ltd., DongGuan City Guangdong Province, China) infrared thermometer (pyrometer). The irradiated samples were annealed at the temperature of 300 °C.

2.2.2. X-ray Phase Analysis

X-ray phase analysis was carried out on a DRON-3 X-ray diffractometer with a CuKα-anode (λ = 1.5418 Å) and Ni-filter using the powder method (Debye-Scherrer polycrystal). The spectrum was recorded with an ionization counter MSTR-4 at angles 4–64°. Radiographs were processed using the software Crystallographica Search-Match Version 2.0.3.1 using the card index data (PDF-4+) of the International Centre for Diffraction Data JCPDS. The phase composition was determined by analyzing the interplanar distance (d) and the intensity of the spectral reference lines.

2.2.3. Electron Microscopy

The microstructure of materials was studied via scanning electron microscopy (SEM) on a high-resolution scanning electron microscope TESCAN MIRA 3 LMU (Tescan, Brno, Czech Republic) in secondary electron modes (SE) and backscattering of electrons (BSE).

Magnification was up to 1 million times. The microscope was equipped with an Energy-dispersive X-ray spectrometer (EDX)- spectrometer Ultim Max 63.

2.2.4. IR Spectroscopy

IR spectra of light absorption by materials were obtained on a Bruker Optics GmbH FTIR spectrometer in the frequency range 4000–400 cm^{-1} (accuracy 0.1 cm^{-1}). The samples were taken in transparent tablets with KBr.

3. Results and Discussion

3.1. Simulation of Fast Electron Passage

The scattering of the fast electrons inside a solid body is calculated using the Rao-Sahib-Whitry model [17], which is a modification of the classical theory of charged particle scattering in matter (the Bethe–Bloch model) [18]. Electrons moving in the material experience primarily ionization and radiation losses [19].

Figure 2 shows the calculations of the dependence of specific ionization and radiation losses of fast electrons in the SC material on the kinetic energy of the electron in the range of 0.1–10.0 MeV, as well as the contribution of each element to the ionization and radiation losses. The calculated ionization and radiation losses of electron energy are $\left(-\frac{dE}{dx}\right)_{col}^{10MeV} = 4.3$ and $\left(-\frac{dE}{dx}\right)_{rad}^{10MeV} = 0.57$, respectively.

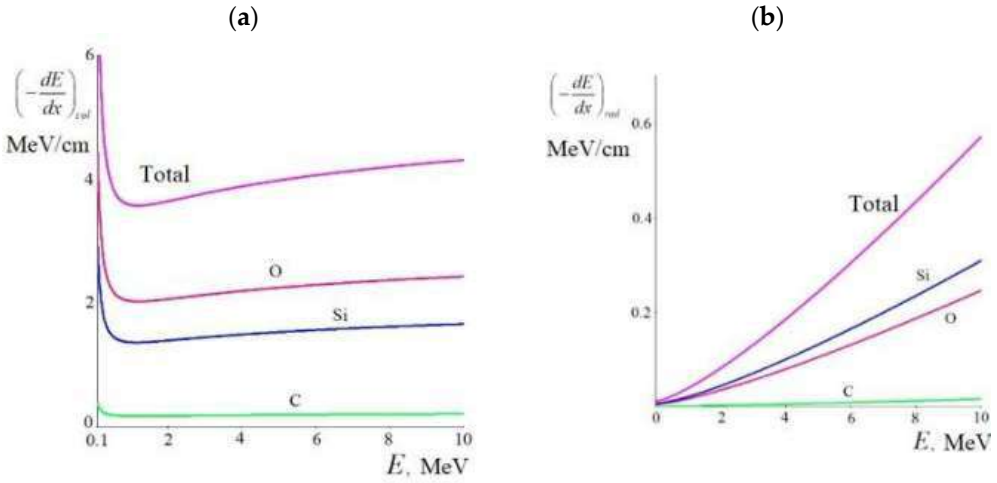

Figure 2. Dependence of specific ionization losses (**a**) and specific radiation losses (**b**) of fast electrons in SC-material on electron kinetic energy (upper curve—total contribution of elements).

It can be seen that silicon and oxygen in ionization and radiation losses make up the main contribution, with oxygen making a greater contribution in ionization losses and silicon making a greater contribution in radiation losses.

Thus, at energies of fast electrons E = 10 MeV and lower, the main contribution to the total energy losses of electrons is made with ionization losses, which are 7.5 times greater than radiation losses.

The total energy losses in the material under study are defined according to Equation (1) and shown in Figure 3.

$$\left(-\frac{dE}{dx}\right) = \left(-\frac{dE}{dx}\right)_{col} + \left(-\frac{dE}{dx}\right)_{rad} \quad (1)$$

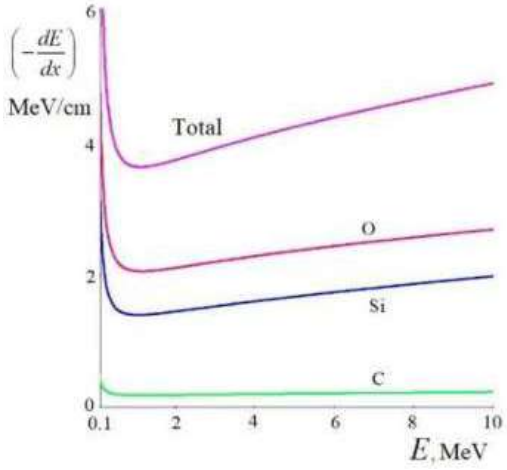

Figure 3. Dependence of total specific energy losses of fast electrons in SC-material on the initial kinetic energy of electrons.

Since the loss of energy of the electron in the material leads to its deceleration, we determined the effective range that the particle would pass during deceleration in an unbounded and homogeneous medium, assuming that it continuously lost energy along the whole path according to the stopping power ($-dE/dx$). The true paths are random and distributed around the effective range, which is calculated using Equation (2) as follows [17]:

$$R(E_0) = \int_0^{E_0} \frac{dE_k}{\left(-\frac{dE}{dx}\right)} \quad (2)$$

With an initial electron energy of 10 MeV, the average range in the studied composite is R (10 MeV) = 23 mm (Figure 4). The spatial distribution of primary and secondary electrons with energies of 10 MeV via the SC material was simulated using the Monte Carlo method [19]. The simulation was performed for 10,000 primary electrons (Figure 5).

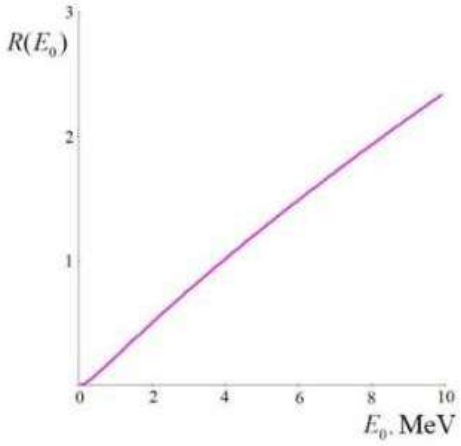

Figure 4. The dependence of the electron effective range in the SC material on its initial kinetic energy.

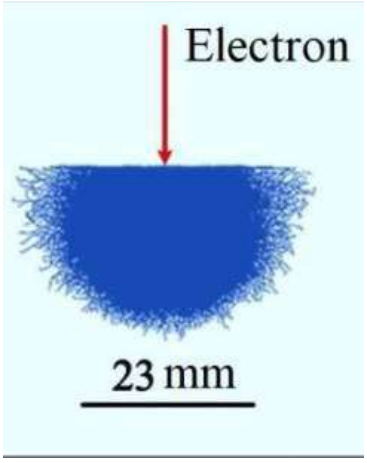

Figure 5. Trajectory of electrons' motion (E = 10 MeV) inside the SC material.

The curves that describe the transmittance factors by the number and the energy of electrons (E = 10 MeV) for normal electron incidence on the surface (φ = 0) are shown in Figure 6.

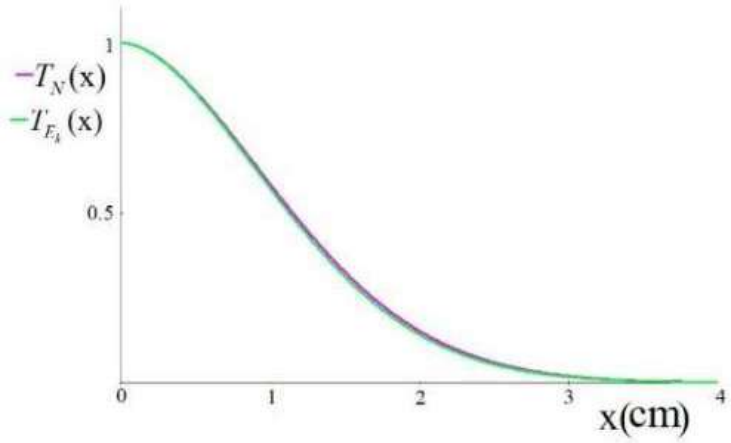

Figure 6. Transmission factors by number and energy of electrons E_0 = 10 MeV for normal electron incidence on the surface (φ = 0).

3.2. Electron Activation of Mineral Phases in the System $Si_xC_yO_z$

One of the promising ways to modify the Si-C system is the method of electron irradiation. The source of the formation of Si clusters is SiO_2 irradiated via fast electrons as a result of its radiation and local heating [7,20]. The peculiarity of electron irradiation is the rapid deceleration of electrons in the material as a result of intense energy exchange with solid-state electrons due to ionization and radiation losses. Electron irradiation with energy less than 1 MeV is characterized by a low level of damage to the crystal lattice structure with unchanged chemical composition in contrast to the effects of other high-energy particles (protons, neutrons, and ions). However, such electrons can initiate chemical reactions.

The irradiation of the materials with energy above 1 MeV leads to the breaking of the chemical bonds of chemical compounds, the ionization of atoms, and the formation of point paramagnetic radiation defects (RD) on the bridging atoms of silicon and oxygen in siloxane (≡Si-O-Si≡) bond and carbon atoms (≡ Si•; ≡ Si-O•; and ≡ C•) [14,21,22]. RDs are also produced in the form of charged V_{Si} and V_C vacancies of atoms as a result of moving an atom (ion) from a crystal lattice node to an inter-node and their complexes [14,21,22]. At the same time, significant structural changes are observed in the amorphous-crystalline lattices of mineral phases based on silicon and carbon.

The V_{Si} and V_C vacancies formed in the materials during high-energy electron irradiation have high mobility with an increased energy level and, therefore, are metastable. Under certain energy conditions, radicals and vacancies on Si and C atoms can transform into less mobile RD complexes in the system (SiO_2-Si-C), which can promote the formation of SiC silicon carbide via the donor–acceptor interaction of activated Si and O atoms [22–27].

The considered defect formation schemes are quite realizable in the synthesized material, which includes silicate and carbon matrices.

3.3. X-ray Diffraction Studies

Figure 7 shows the diffractogram of the X-ray phase analysis of the synthesized silicate-carbon material. The diffractogram of the powdered (dispersibility 0.1–0.15 μm) material corresponds to the amorphous–crystalline state of the components in this material, as evidenced by two intense and broadened amorphous halos in the Bragg angle region 2θ = 7–11° and 18–25° (Figure 7).

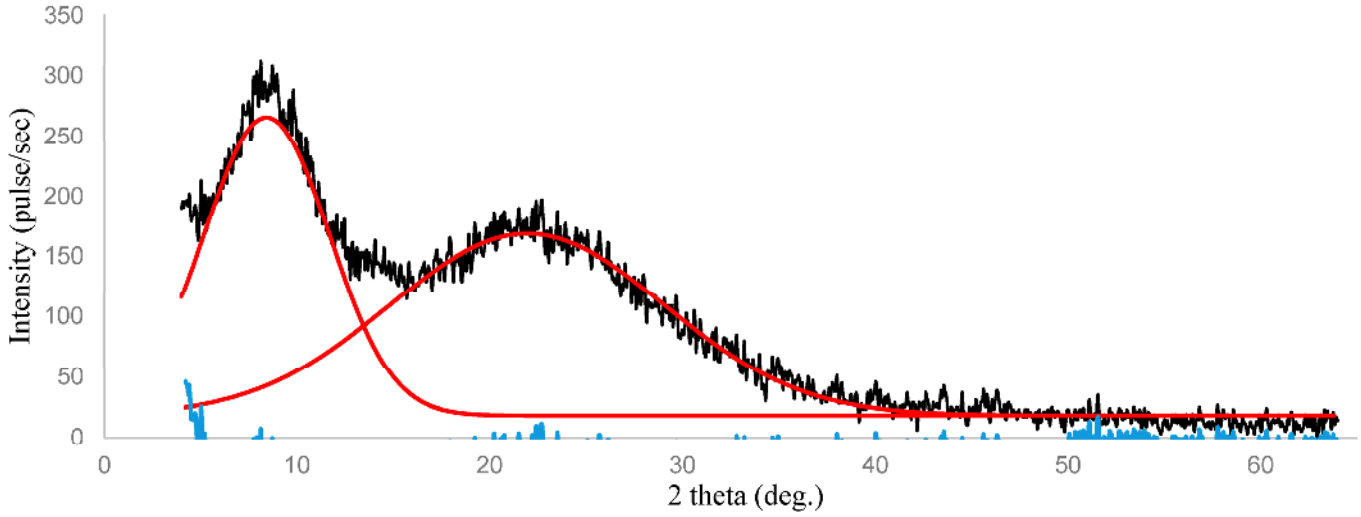

Figure 7. X-ray phase analysis of SC material after ultrasonic treatment (before irradiation).

The black color on the X-ray diffraction patterns represents the original spectrum of the sample; the red color shows the areas characterizing the amorphous phase, obtained using the regression analysis Gaussian model; the blue color shows the spectrum of the crystalline phase obtained by subtracting the region of the amorphous phase from the original spectrum.

Amorphous halo in the area 2θ = 18–25° corresponds to the formation of highly dispersed amorphous silica according to PDF 01-075-3159. The proportion of amorphized silica was about 90%.

An amorphous halo in the area 2θ = 7–11° is not characteristic of silica and may correspond to the formation of a carbon structure in the material, which is close to the graphitopod phase or graphite oxide. The crystalline phase in area 7–11° (d = 10.901; 10.463; 9.425; 8.400 Å) is typical for graphite oxide (GO) with crystallographic index 002 [28]. Graphite oxide is a product of variable composition consisting of hydrophilic layers (d = 6–12 Å) and intercalated water molecules [24].

The effect of the formation of carbon structures in the silicate matrix can be the result of the pyrolysis of hydrocarbon (CH_3-, C_2H_5-) radicals in the polyalkylhydrosiloxane oligomer and the recombination of radicals, for example, via the following reaction:

$$2(CH_3)_{gas} \rightarrow 3H_2 + 2C_{solid}$$

with the subsequent condensation of carbon on amorphous silica.

Irradiation with electrons with an absorbed dose of 10^5 MGy or less does not lead to any changes in the properties of the silicon–carbon powder according to X-ray phase and IR-Fourier spectroscopic analysis.

As a result of the electron irradiation (D = 10^6 Gy) of the material significant structural-phase transformations were observed. (Figures 8 and 9). Also, as in Figures 7–9 show the original spectrum of the sample in black on the X-ray patterns; the red color shows the areas characterizing the amorphous phase, obtained by regression analysis Gaussian model; the blue color shows the spectrum of the crystalline phase obtained by subtracting the region of the amorphous phase from the original spectrum. There was an increase in intensity in the region of 2θ = 18–25° (corresponding to silica PDF number 51-1377) by 25–30% on the X-ray diffraction pattern (Figure 8) and a decrease in the line half-width (Δ = 2.0°). This fact indicated the partial crystallization of amorphous SiO_2.

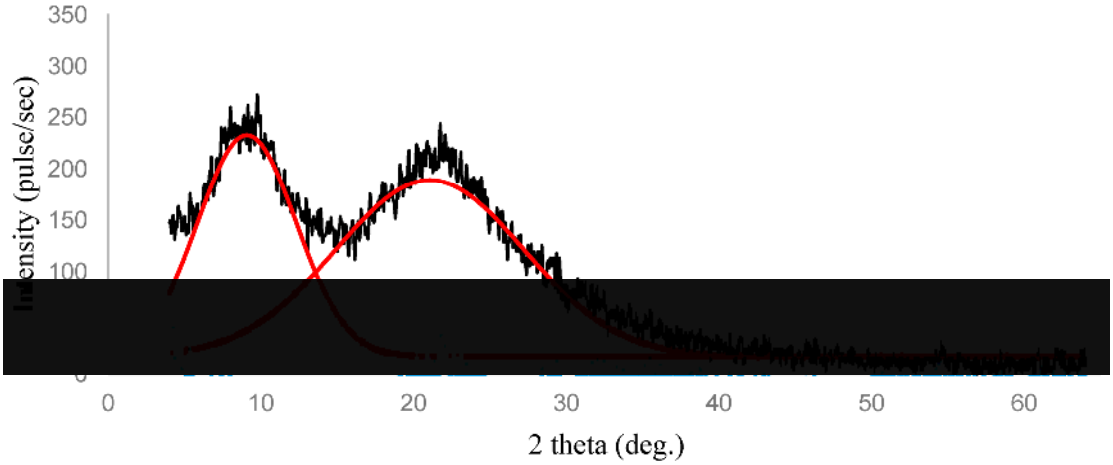

Figure 8. X-ray phase analysis of SC material after electron irradiation (D = 10^6 Gy).

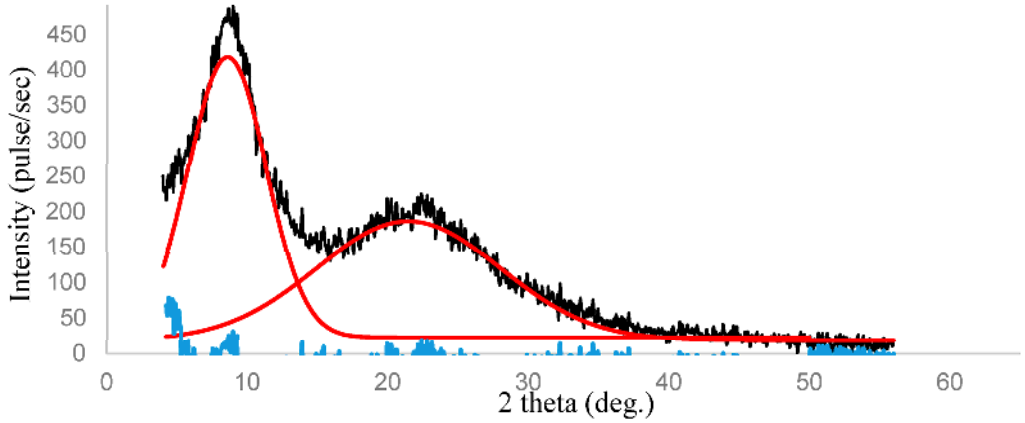

Figure 9. X-ray phase analysis of SC material after electron irradiation (D = 10^7 Gy).

At the same time, a slight increase in the intensity of the amorphous halo was observed in the region 2θ = 7–11° by 12–15% on the X-ray diffraction pattern (Figure 8), which can be attributed to a graphite-like phase or graphite oxide.

Thus, the start of induced crystallization of SiO_2 was observed during electron irradiation (D = 10^6 Gy). The formation of a small number of crystals of low-temperature tetragonal β-cristobalite SiO_2 (2θ = 22.4°, d = 4.086 Å) was recorded [9–11,29]. Clear Bragg lines at d = 3.339; 3.132; 2.290; 1.821; 1.668 Å, corresponding to β-cristobalite, are also fixed [14,30]. It should be noted that, according to the literature data, the formation of cristobalite (JCPDS 39-1425) from a polyalkylhydrosiloxane oligomer is possible during heat treatment at 1300–1400 °C in an electric furnace [31,32]. And in our study, the same

results were obtained during thermal treatment at 300 °C with further electron irradiation. Irradiation with electrons can lead to the formation of defects in the structure of silicon oxide, and radiation damage will serve as crystallization nuclei [4,5,9]. As a result, crystallization can take place during low-temperature electron irradiation.

Our studies showed that the temperature of the material irradiated by fast electrons did not exceed 150 °C. Consequently, the structural-phase transformations and dissociation of SiO_2 during its irradiation with fast electrons can occur in the near-surface layers of silica.

The presence of the C-phase in the structure of the material contributes to an increase in thermal conductivity and, as the experiment showed, contributes to the crystallization of SiO_2.

An increase in the absorbed dose of fast electrons from D = 10^6 to D = 10^7 Gy leads to the opposite effect (Figure 9). The amorphization of silica is observed, as evidenced by a sharp broadening of the diffraction region at 2θ = 18–25°. At the same time, the intensity decreases by only 7–9%. On the diffractogram of the material after irradiation with an absorbed dose of 10^7 MGy (Figure 9), a sharp increase in the intensity (by 55–60%) of the diffraction region at 2θ = 7–11° attracts attention. This fact may indicate the recrystallization of mineral phases with a high degree of crystal defects.

3.4. Morphology of Mineral Phases

The morphology of the mineral phase particles in the material was studied via scanning electron microscopy (SEM). The initial material contains the following (Figure 10):

(1) Polydisperse conglomerate grains with distinct facets of different shapes from 1 μm to 15 μm, consisting of small crystallites ranging in size from 0.2 μm to 3.5 μm, which correspond to crystalline silica (Figure 10a,b).
(2) Spherical particles ranging in size from 0.1 μm to 2.0 μm, which correspond to amorphous silica. The particles have a smooth surface without pores or cracks. The surface of larger particles is covered with white agglomerates (Figure 10c,d).
(3) Irregularly shaped plate formations up to 0.1 μm thick, which correspond to the structure of the graphite-like phase. On the surface of the plates, there were nanoparticles sized 20–30 nm, which corresponds to ~(40–75 nm) graphene layers in the stacks (Figure 10c,d).

The morphology of the surface of electron-irradiated SC-material particles underwent significant structural changes (Figures 11 and 12). Irregularly shaped silica crystals with distinct faces were formed. The size of silica agglomerates increased up to 35 μm with the fixation of quasi-spherical particles 0.5–0.7 μm in diameter with smooth surfaces without pores and cracks on the surface (Figure 11a,b). The microphotograph of the section of the graphite-like particle plane clearly shows a solid gray silica film about 2 μm thick with spherical particles sized 0.5–2.5 μm embedded (Figure 11d).

The irradiation of the material with an electron beam with an absorbed dose of D = 10^7 Gy (Figure 12) leads to the intensive formation of smaller spherical particles on silica ranging in size from 20 nm to 160 nm as well as the formation of whiskers.

Additional information on the composition and structure of the mineral phases in the material subjected to pyrolysis and electron irradiation is provided in the IR spectroscopy data.

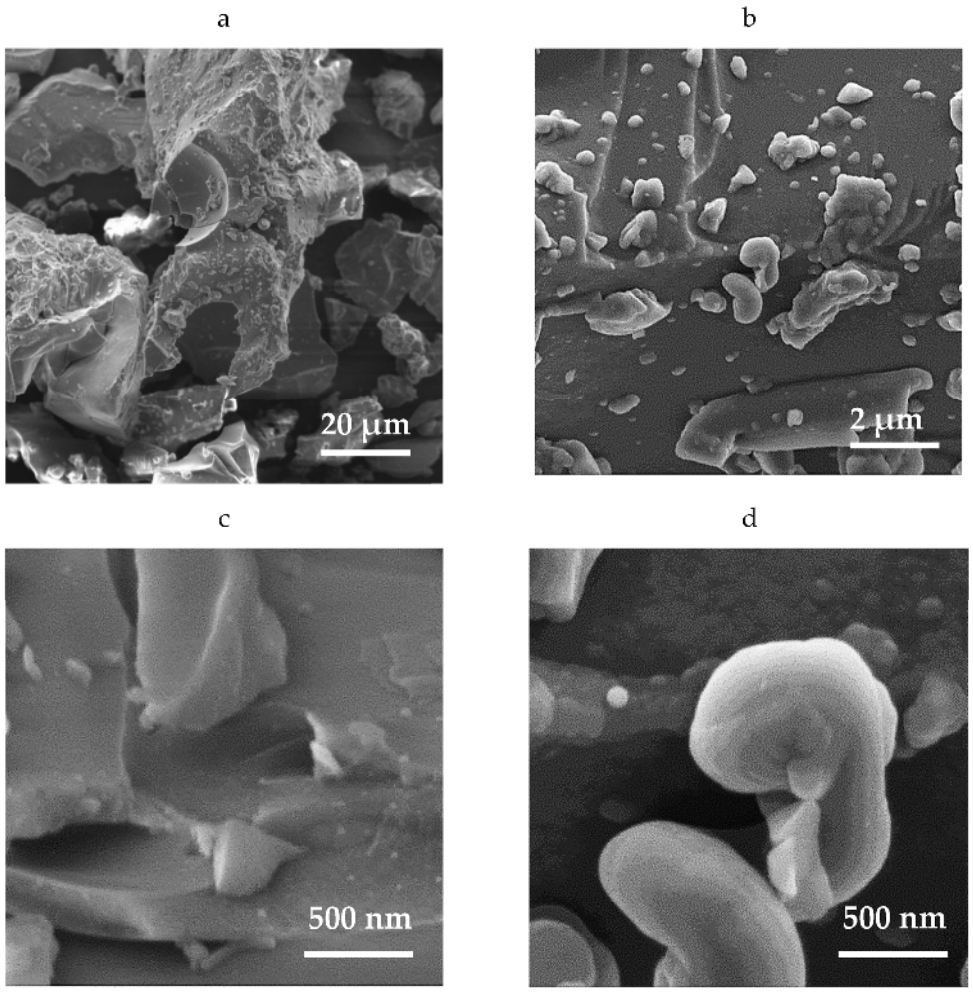

Figure 10. Microstructure of the original SC material (before electron processing): (**a**) $\times 5.7 \times 10^3$, (**b**) $\times 5.7 \times 10^4$, (**c**,**d**) $\times 28.5 \times 10^4$.

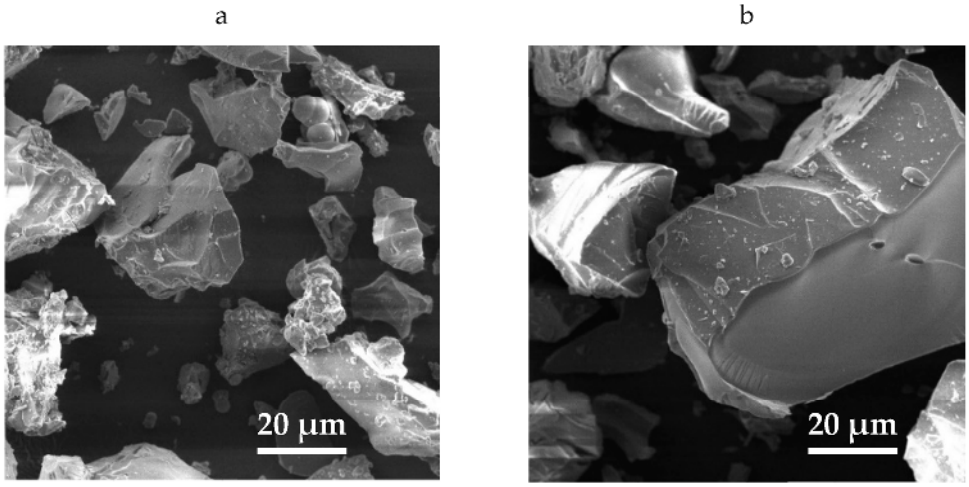

Figure 11. *Cont.*

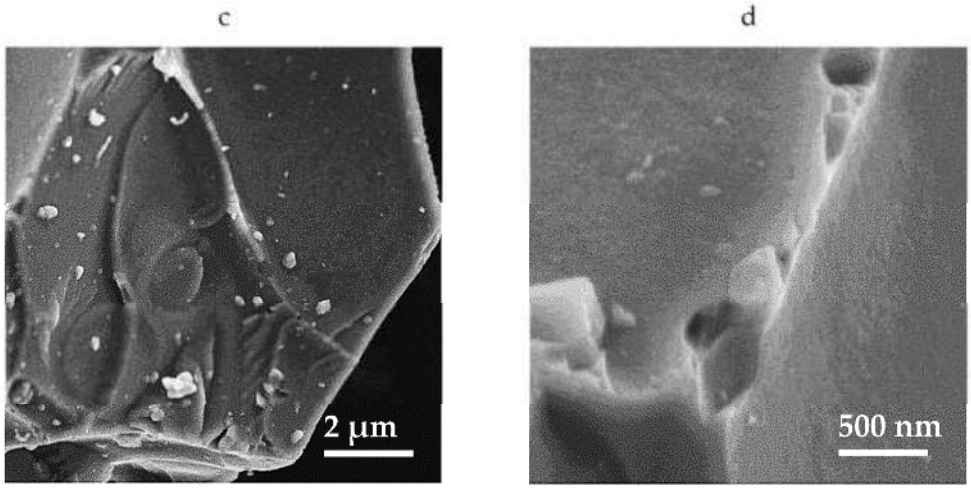

Figure 11. Microstructure of the SC material exposed to electron irradiation (E = 10 MeV; D = 10^6 Gy): (**a**,**b**) ×5.7 × 10^3, (**c**) ×5.7 × 10^4, (**d**) ×28.5 × 10^4.

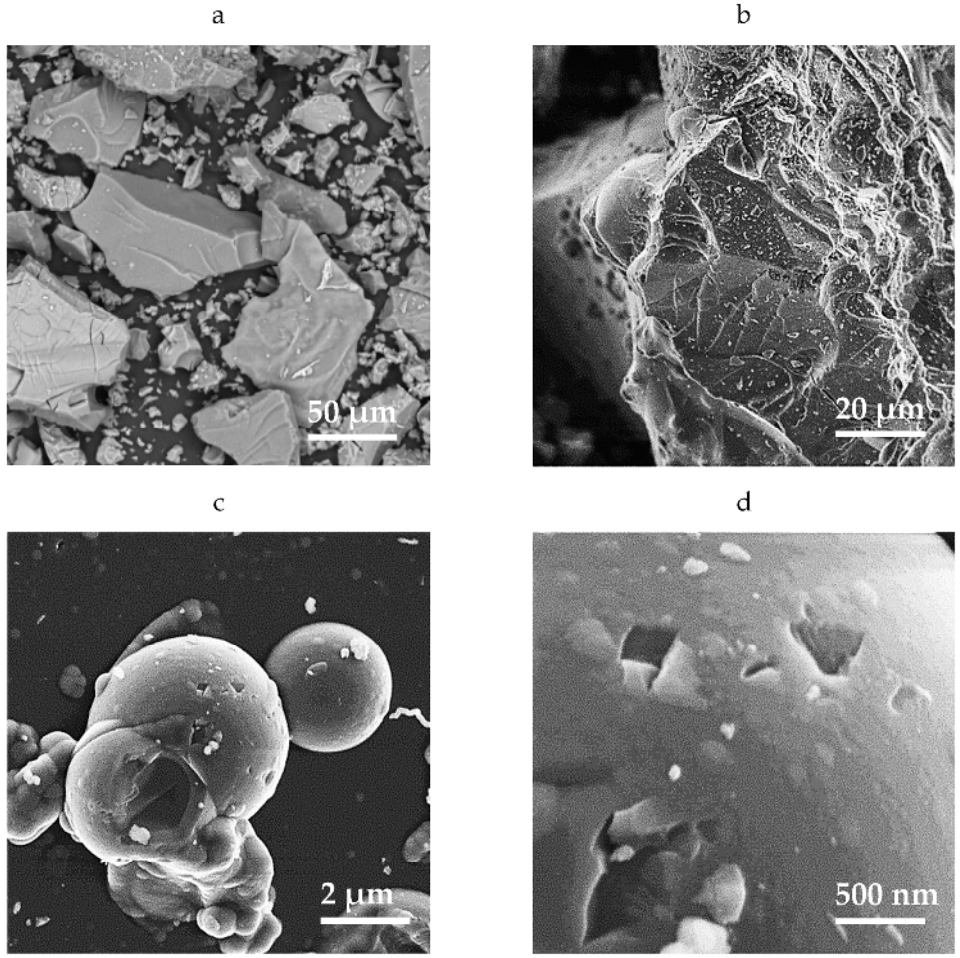

Figure 12. Microstructure of the SC material exposed to electron irradiation (E = 10 MeV; D = 10^7 Gy): (**a**) ×2.28 × 10^3, (**b**) ×5.7 × 10^3, (**c**) ×5.7 × 10^4, (**d**) ×28.5 × 10^4.

3.5. IR Spectroscopic Studies

In the infrared spectrum of the initial material, we observed intense absorption bands with maximums at 1039 cm^{-1} and 780 cm^{-1}, which, respectively, can be attributed to the predominantly valence antisymmetric and symmetric vibrations of the bridging siloxane

(≡Si-O-Si≡)-groups, as well as deformation vibrations at 455 cm^{-1} to the silicon–oxygen groups (Figure 13) [33].

The peculiarity of this spectrum is the presence of an absorption band at 598 cm^{-1}, referred to symmetrical (≡Si-O-Si≡)- vibrations of silica-oxygen [SiO_4]- tetrahedrons. There is also an intense absorption band in the area of 1200–1100 cm^{-1}, characteristic of amorphous hydroxylated silica. The amorphous nature of silica is indicated by the broadening of these absorption bands.

The formation of C-phases (or graphite oxide) in the silicate matrix during the pyrolysis of the polyalkylhydrosiloxane oligomer resulted in the appearance of two absorption bands at 1276 and 1420 cm^{-1} in the spectrum, which are attributed to the C-O-C and C-O bonds with an amorphous structure. It can be assumed that the formation of these bonds confirms the X-ray phase analysis data on the formation of a graphite-like phase oxide (GO) in the system as a result of breaking the C-C bonds and their oxidation during the pyrolysis of the polyalkylhydrosiloxane oligomer.

Electron irradiation of the material introduces a change in the IR spectrum. In the spectrum of the SC material exposed to fast electrons, clear and intense absorption bands were observed (≡Si-O-Si≡). Thus, the main absorption band at 1039 cm^{-1} (before irradiation) slightly shifted to the low-frequency area (up to 1038 cm^{-1}) after exposure to fast electrons (D = 10^6 Gy) and shifted markedly to the high-frequency area (isochoric shift) when irradiated with fast electrons (D = 10^7 Gy) to 1045 cm^{-1}. The latter circumstance indicated an increase in the strength of the Si-O bond and an increase in the degree of polymerization [SiO_4]- tetrahedrons as a result of electron-induced crystallization [34].

The absorption band at 1097 cm^{-1}, characteristic of amorphous hydroxylated silica (before irradiation) also shifted to the high-frequency area of the spectrum, up to 1115 cm^{-1} during electron irradiation (D = 10^6 Gy). Electron irradiation at increased absorbed dose (D = 10^7 Gy), and the intensity of the absorption bands in the spectrum decreased markedly (by 60–68%), which indicates the course of defect formation and amorphization of the silicate matrix [34,35].

In the process of electron irradiation of the material, attention is drawn to the change in the ratio of the intensity of the main absorption bands of the siloxane bond of the valence (γ_{as}) at 1115 cm^{-1} and deformational (δ)-oscillations at 455 cm^{-1}: from $I(\gamma_{as})/I(\delta)$ = 3.1 (before irradiation) to 8.6 (after irradiation at D = 10^6 Gy). This indicated stabilization of vibrations through deformation angles in the siloxane bond and an increase in vibrations through valence bonds with an increase in the molecular weight of siloxane as a result of an increase in its degree of polymerization and the rigidity of siloxane chains under electron impact.

In general, a silicate matrix irradiated by fast electrons (D = 10^7 Gy) is largely amorphized (band broadening to Δ150 cm^{-1}). There was a sharp decrease in the ratio of $I(\gamma_{as})/I(\delta)$ = 2.7. This indicates an increase in the vibration of siloxane chains, on the contrary, with deformation angles and thereby increasing their flexibility with a possible decrease in the molecular weight of the silicate as a result of breaking the siloxane bond (≡Si-O-Si≡).

In the infrared spectrum of the initial material, absorption bands in the area of 3600–3400 cm^{-1} and at 1635 cm^{-1} belong, respectively, to the valence and deformation vibrations of adsorbed and coordinately bound water (hydroxyl OH-groups) [11]. Apparently, there are several structurally non-equivalent OH-groups in the silica-oxygen mesh of the material, forming bonds of different strengths in the polycondensation reactions and the construction of a three-dimensional silica-oxygen framework. Electron irradiation (D = 10^6 Gy) on the surface of the material particles led to the formation of the same type of OH-groups.

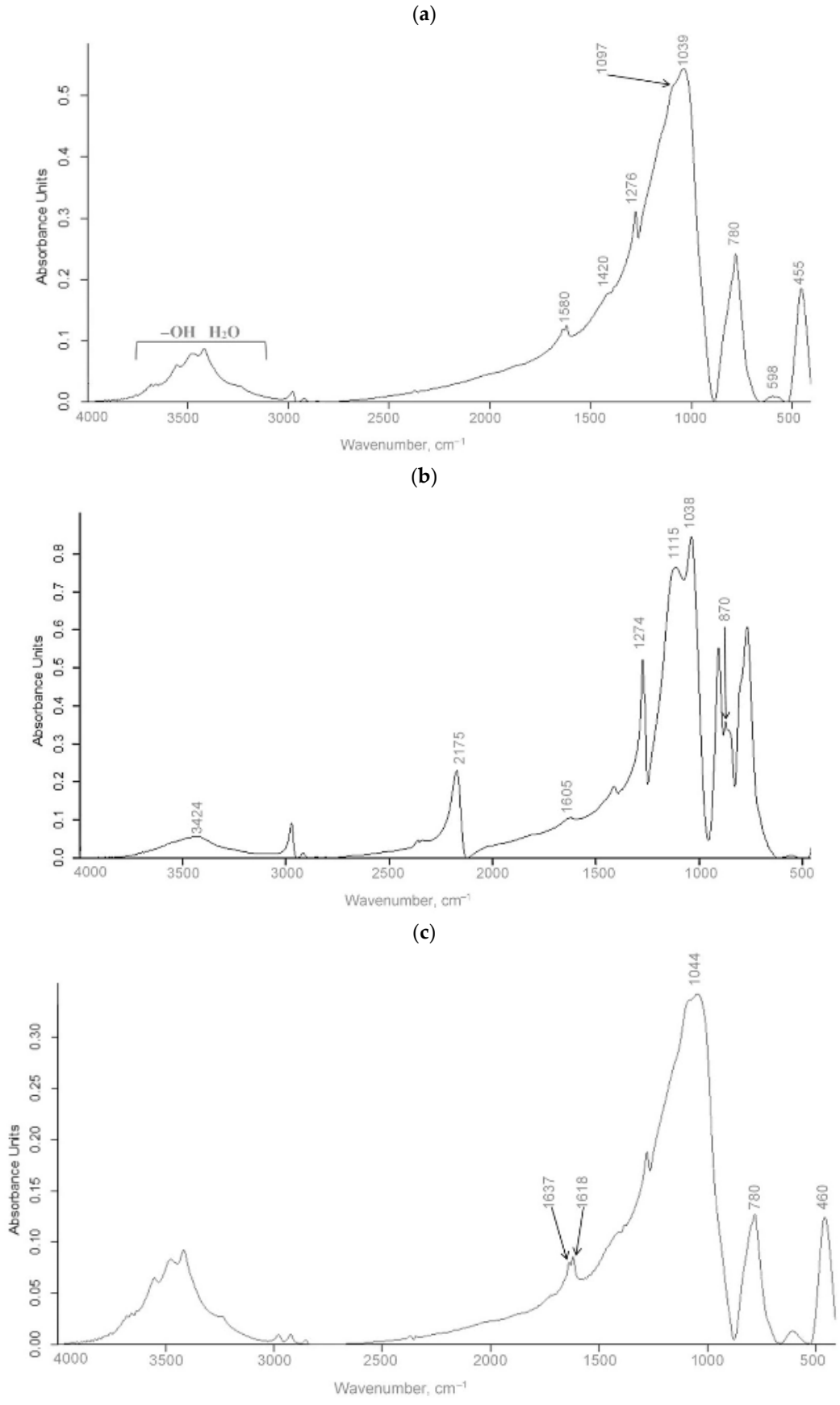

Figure 13. IR spectra of SC material before irradiation (**a**) and after electron irradiation: D = 10^6 Gy (**b**) and D = 10^7 Gy (**c**).

4. Conclusions

The principal possibility of obtaining nanodispersed amorphous-crystalline SiO_2 modified with graphite-like structures from polyalkylhydrosiloxane oligomers with high active hydrogen content at a reduced pyrolysis temperature (300 °C) has been established.

Irradiation via fast electrons with energy 10 MeV and absorbed dose 10^6 Gy leads to structural-phase transformations in the material. There was an increase in intensity in the region 2θ = 18–25° (corresponding to silica) by 25–30% on the X-ray diffraction pattern and a decrease in the line half-width (Δ = 2.0°). This fact indicated the crystallization of amorphous SiO_2.

An increase in the absorbed dose of fast electrons from D = 10^6 to D = 10^7 Gy leads to the opposite effect. The amorphization of silica is observed, as evidenced by a sharp broadening of the diffraction region at 2θ = 18–25°. At the same time, the intensity decreases by only 7–9%. On the diffractogram of the material after irradiation with an absorbed dose of 10^7 MGy, a sharp increase in the intensity (by 55–60%) of the diffraction region at 2θ = 7−11° attracts attention, which can be attributed to a graphite-like phase or graphite oxide.

Further research should be continued to expand the boundaries of optimal absorbed radiation doses of fast electrons to achieve the maximum crystallization effect of the silicon–carbon powder.

Author Contributions: Conceptualization, V.I.P.; Formal analysis, O.D.E.; Funding acquisition, V.I.P.; Investigation, A.V.N., D.S.P. and A.O.P.; Methodology, R.N.Y. and A.I.G.; Validation, R.N.Y. and A.I.G.; Writing—original draft, V.I.P.; Writing—review and editing, N.I.C. All authors have read and agreed to the published version of the manuscript.

Funding: This work was realized using the equipment of the High Technology Center at BSTU, named after V.G. Shukhov, the framework of the State Assignment of the Ministry of Education and Science of the Russian Federation, project No. FZWN-2023-0004.

Data Availability Statement: Data sharing not applicable.

Conflicts of Interest: The authors declare no conflict of interest. The funders had no role in the design of this study; in the collection, analyses, or interpretation of data; in the writing of the manuscript, or in the decision to publish the results.

References

1. Pavlenko, V.I.; Cherkashina, N.I. Effect of SiO_2 crystal structure on the stability of polymer composites exposed to vacuum ultraviolet radiation. *Acta Astronaut.* **2019**, *155*, 1–9. [CrossRef]
2. Du, B.; Hong, C.; Zhang, H.; Wang, J.; Qu, Q. Preparation and mechanical behaviors of SiOC-modified carbon-bonded carbon fiber composite with in-situ growth of three-dimensional SiC nanowires. *J. Eur. Ceram. Soc.* **2018**, *38*, 2272–2278. [CrossRef]
3. Jayalath, S.; Herath, M.; Epaarachchi, J.; Trifoni, E.; Gdoutos, E.E.; Fang, L. Durability and long-term behaviour of shape memory polymers and composites for the space industry—A review of current status and future perspectives. *Polym. Degrad. Stab.* **2023**, *211*, 110297. [CrossRef]
4. Baranov, E.A.; Konstantinov, V.O.; Shchukin, V.G.; Zamchiy, A.O.; Merkulova, I.E.; Lunev, N.A.; Volodin, V.A. Electron-Beam Crystallization of Thin Films of Amorphous Silicon Suboxide. *Tech. Phys. Lett.* **2021**, *47*, 263–265. [CrossRef]
5. Shuleiko, D.V.; Kashaev, F.V.; Potemkin, E.V.; Zabotnov, S.V.; Zoteev, A.V.; Presnov, D.E.; Parkhomenko, I.N.; Romanov, I.A. Structural Anisotropy of Amorphous Silicon Films Modified by Femtosecond Laser Pulses. *Opt. Spectrosc.* **2018**, *124*, 801–807. [CrossRef]
6. Song, L.W.; Zhan, X.D.; Benson, B.W.; Watkins, G.D. Bistable interstitial-carbon–substitutional-carbon pair in silicon. *Phys. Rev. B* **1990**, *42*, 5765. [CrossRef] [PubMed]
7. Yoshida, A.; Kaburagi, Y.; Hishiyama, Y. Full width at half maximum intensity of the G band in the first order Raman spectrum of carbon material as a parameter for graphitization. *Carbon* **2006**, *44*, 2333–2335. [CrossRef]
8. Bereznyak, E.P.; Borts, B.V.; Sayenko, L.A. The effect of electron irradiation on structural-phase state of rock-forming quartz. *Probl. At. Sci. Technol.* **2012**, *5*, 8–12.
9. Kim, C.; Lim, S.; Jeong, C. Ultrafast crystallization of amorphous silicon thin films by using an electron beam annealing method. *J. Korean Phys. Soc.* **2014**, *64*, 1091–1095. [CrossRef]
10. Kalanov, M.U.; Khugaev, A.V. α–β Phase Transition in the Impurity Phase of a SiO_2 Single Crystal. *Tech. Phys. Lett.* **2021**, *47*, 349–352. [CrossRef]

11. Dimova-Malinovska, D. Polycrystalline Si films prepared by Al- and Ni-induced crystallization. *J. Optoelectron. Adv. Mater.* **2005**, *7*, 99–106.
12. Kompan, M.E.; Krylov, D.S.; Sokolov, V.V. Raman scattering in self-formed nanoporous carbon produced on the basis of silicon carbide. *Semiconductors* **2011**, *45*, 306–311. [CrossRef]
13. Zamchiy, A.O.; Baranov, E.A.; Merkulova, I.E.; Lunev, N.A.; Volodin, V.A.; Maksimovskii, E.A. Indium-Induced Crystallization of Thin Films of Amorphous Silicon Suboxide. *Tech. Phys. Lett.* **2020**, *46*, 583–586. [CrossRef]
14. Youn, R.C.; Corelli, J.C. Photoconductivity Studies of Radiation-Induced Defects in Silicon. *Phys. Rev. B* **1971**, *5*, 1455–1467. [CrossRef]
15. Li, X.; He, Y.; Talukdar, S.S.; Swihart, M.T. Process for Preparing Macroscopic Quantities of Brightly Photoluminescent Silicon Nanoparticles with Emission Spanning the Visible Spectrum. *ACS Publ. Most Trust. Most Cited. Most Read* **2003**, *19*, 8490–8496. [CrossRef]
16. Ehbrecht, M.; Huisken, F. Gas-phase characterization of silicon nanoclusters produced by laser pyrolysis of silane. *Phys. Rev. B* **1999**, *59*, 2975–2985. [CrossRef]
17. Rao-Sahib, T.S.; Wittry, D.B. X-ray continuum from thick elemental targets for 10–50-keV electrons. *J. Appl. Phys.* **1974**, *45*, 5060–5068. [CrossRef]
18. Sigmund, P. *Particle Penetration and Radiation Effects*; Springer Series in Solid State Sciences; Springer: Berlin/Heidelberg, Germany, 2006; Volume 151.
19. Kotera, M.; Murata, K.; Nagami, K. Monte Carlo simulation of 1–10-KeV electron scattering in a gold target. *J. Appl. Phys.* **1981**, *52*, 997–1003. [CrossRef]
20. Zickler, G.A.; Smarsly, B.; Gierlinger, N.; Peterlik, H.; Paris, O. A reconsideration of the relationship between the crystallite size La of carbons determined by X-ray diffraction and Raman spectroscopy. *Carbon* **2006**, *44*, 3239–3246. [CrossRef]
21. Denisyuk, I.Y.; Logushkova, K.Y.; Fokina, M.I.; Uspenskaya, M.V. FT-IR-Spectra of Multilayered Graphene and Its Composition with Surface-Active Material. *Opt. Spectrosc.* **2018**, *125*, 918–920. [CrossRef]
22. Bakaleinikov, L.A.; Zamoryanskaya, M.V.; Kolesnikova, E.V.; Sokolov, V.I.; Flegontova, E.Y. Silicon dioxide modification by an electron beam. *Phys. Solid State.* **2004**, *46*, 1018–1023. [CrossRef]
23. Ghara, M.; Pan, S.; Chattaraj, P.K. Donor–Acceptor vs Electron-Shared Bonding: Triatomic Si_nC_{3-n} ($n \leq 3$) Clusters Stabilized by Cyclic Alkyl(amino) Carbene. *ACS Publ. Most Trusted. Most Cited. Most Read* **2019**, *123*, 10764–10771. [CrossRef] [PubMed]
24. Moll, M.; Fretwurst, T.; Kuhnke, M.; Lindström, G. Relation Between Microscopic Defects and Macroscopic Changes in Silicon Detector Properties after Hadrons Irradiation. *Nucl. Instrum. Methods Phys. Res. B* **2002**, *186*, 100–110. [CrossRef]
25. Asghar, M.; Iqbal, M.; Zafar, N. Characterization of deep levels introduced by alpha radiation in *n*-type silicon. *J. Appl. Phys.* **1993**, *73*, 3698–3708. [CrossRef]
26. Kyutt, R.N.; Danishevskii, A.M.; Smorgonskaya, É.A.; Gordeev, S.K. X-raying studies of the nanoporous carbon structure produced from carbide materials. *Semiconductors* **2003**, *37*, 784–788. [CrossRef]
27. Morozov, V.N.; Smirnova, E.V. The infrared spectra of single-crystal and polycrystalline films on fused quartz. *J. Appl. Spectrosc.* **1974**, *20*, 506–508. [CrossRef]
28. Sidorov, A.I.; Leks, E.Y.; Podsvirov, O.A.; Vinogradov, A.Y. Crystallization and silicon carbide formation in two-layer amorphous silicon-carbon films during electron irradiation. *Tech. Phys.* **2022**, *11*, 1475. [CrossRef]
29. Galyshev, S.; Postnova, E.; Shakhlevich, O.; Agarkov, D.; Agarkova, E.; Nekrasov, A.; Mozhchil, R. Heat Treatment Effect on the Phase Composition of the Silica Electrochemical Coating and the Carbon Fiber Strength. *Materials* **2021**, *14*, 5209. [CrossRef]
30. Coh, S.; Vanderbilt, D. Structural stability and lattice dynamics of SiO_2 cristobalite. *Phys. Rev. B* **2008**, *78*, 054117. [CrossRef]
31. Zhu, W.; Guo, A.; Xue, Y.; Zhang, J.; Liu, Z.; Cao, C.; Zhang, F.; Liu, J. Mechanical evaluations of mullite fibrous ceramics processed by filtration and in situ pyrolysis of organic precursor. *J. Eur. Ceram. Soc.* **2019**, *39*, 1329–1335. [CrossRef]
32. He, C.; Liu, X.; Ma, C.; Cao, Y.; Hou, F.; Yan, L.; Guo, A.; Liu, J. Digital light processing of Si-based composite ceramics and bulk silica ceramics from a high solid loading polysiloxane/SiO_2 slurry. *J. Eur. Ceram. Soc.* **2021**, *41*, 7189–7198. [CrossRef]
33. Shamin, S.N.; Galakhov, V.R.; Aksenova, V.I.; Karpov, A.N.; Shvartz, N.L.; Yanovitskaya, Z.S.; Volodin, V.A.; Antonova, I.V.; Ezhevskaya, T.B.; Jedrzejewski, J.; et al. X-ray and infrared spectroscopy of layers produced by cosputtering of spatially separated SiO_2 and Si sources. *Semiconductors* **2010**, *44*, 531–536. [CrossRef]
34. Yoon, S.Y.; Park, S.J.; Kim, K.H.; Jang, J. Metal-induced crystallization of amorphous silicon. *Thin Solid* **2001**, *383*, 34. [CrossRef]
35. Pezoldt, J. The influence of surface preparation on the properties of SiC on Si. Physica Status Solidi A—Applied Research. *Phys. Status Solidi A* **2001**, *185*, 159–166. [CrossRef]